J. Ocean Univ. China (Oceanic and Coastal Sea Research)
DOI 10.1007/s11802-013-2223-8
ISSN 1672-5182, 2013 12 (2): 230-236
http://www.ouc.edu.cn/xbywb/
E-mail:xbywb@ouc.edu.cn

The Impact of Meso-Scale Eddies on the Subtropical Mode Water in the Western North Pacific

LIU Cong, and LI Peiliang*

Physical Oceanography Laboratory, *Ocean University of China*, *Qingdao* 266100, *P. R. China*

(Received November 16, 2012; revised February 20, 2013; accepted April 7, 2013)

Abstract Based on the temperature and salinity from the Argo profiling floats and altimeter-derived geostrophic velocity anomaly (GVA) data in the western North Pacific during 2002–2011, the North Pacific Subtropical Mode Water (NPSTMW) distribution is investigated and cyclonic and anti-cyclonic eddies (CEs and AEs) are constructed to study the influence of their vertical structures on maintaining NPSTMW. Combining eddies identified by the GVA data and Argo profiling float data, it is found that the average NPSTMW thickness of AEs is about 60 dbar, which is thicker than that of CEs. The NPSTMW thicker than 150 dbar in AEs accounts for 18%, whereas that in CEs accounts for only 1%. About 3377 (3517) profiles, which located within one diameter of the nearest CEs (AEs) are used to construct the CE (AE). The composite AE traps low-PV water in the center and with a convex shape in the vertical section. The 'trapped depth' of the composite CE (AE) is 300 m (550 m) where the rotational velocity exceeds the transitional velocity. The present study suggests that the anticyclonic eddies are not only likely to form larger amounts of NPSTMW, but also trap more NPSTMW than cyclonic eddies.

Key words thickness of NPSTMW; meso-scale eddies; swirl velocity; trapped depth

1 Introduction

NPSTMW is characterized by a pycnostad between the seasonal and main thermoclines in the western part of the North Pacific subtropical gyre (Masuzawa, 1969). It is formed because of the regional wintertime convective cooling (Bingham, 1992; Suga and Hanawa, 1995; Suga *et al.*, 2004). As a minimum potential vorticity (PV) layer, the STMW can be detected over a wide geographic domain from 130°E to the date line and from the Kuroshio-Kuroshio Extension (KE) system to the subtropical countercurrent.

Data analysis and modeling research have been done on the role of meso-scale eddies in the formation, transportation and dissipation of the STMW. Based on Argo profiling float data, Uehara *et al.* (2003) pointed out that anticyclonic meso-scale eddies tend to trap more intense STMW than cyclonic meso-scale eddies. By analyzing historical CTD/XBT data, Qiu and Chen (2006) found that the formation of the STMW is closely associated with the dynamical state of the KE. When the dynamical state is unstable, the KE system will dispatch more cyclonic eddies, carrying the high-PV water to the recirculation gyre and preventing the development of a deep winter mixed layer. By combining satellite-derived sea surface height anomaly data and the Argo profiling float data, the composite distribution of the mixed layer depth (MLD) around the centers of AEs and CEs in the North Pacific Ocean in late winter was analyzed (Kouketsu *et al.*, 2012). The distribution showed that it was more (less) likely to find deeper MLD inside anticyclonic (cyclonic) eddies than outside the eddies.

All the above-mentioned studies focus on the formation of mode waters and suggest that anti-cyclonic meso-scale eddies favor the formation of mode waters comparing to cyclonic eddies. However, it is also very important to reveal the transportation of mode waters and the role that the meso-scale eddies play in the transport. A series of high resolution eddy-resolving ocean general circulation models (OGCM) has been used to investigate eddies' effects on the subduction and distribution of NPSTMW (*e.g.*, Qu *et al.*, 2002; Raninville *et al.*, 2007; Nishikawa *et al.*, 2010). Through analyzing the NPSTMW budget, and the volume and PV budgets between 25.0–25.5σ_0 density layers, Raininville *et al.* (2007) demonstrated that eddies have a dominant role in the transport and distribution of NPMTMW. As shown by Nishikawa *et al.* (2010), a single anticyclonic eddy can trap low PV water in fall and destruct the PV gradient by transporting high (low) PV water to the south (north) on the eastern (western) side in late winter.

In this study, the Argo profiling float data and altimeter data accumulated in the past ten years are used to investigate the vertical structure of the meso-scale eddies. With

* Corresponding author. Tel: 0086-532-66781528
E-mail: lpliang@ouc.edu.cn

the T-S profiles obtained from the KESS program and Hot-spot program, the contribution of meso-scale eddies to NPSTMW is also examined. The paper is organized as follows. In Section 2 the study region and the two data sets (altimetry and Argo data) are described. The eddy identification algorithm from satellite data as well as the methodology used to classify the Argo profiles is also presented in this section. Section 3 describes the characteristics of the STMW in the cyclonic and anti-cyclonic mesoscale eddies, discusses the possible reasons for the differential STMW in cyclonic and anti-cyclonic eddies, and summarizes the study results.

2 Data and Methods

The study region, where the STMW is formed, extends from the Kuroshio-Kuroshio Extension (KE) system (40˚N) to the subtropical countercurrent (20˚N) and from 130˚E to the date line.

2.1 Altimeter-Derived Geostrophic Velocity Anomaly and Eddy Identification

The time delayed daily GVA data, spanning from January 2002 to February 2011, are used to determine the characteristics of meso-scale eddies in the study domain. This gridded altimeter product, produced by Ssalto/Duacs and distributed by Aviso (http://www.aviso.oceanobs.com), provides the best spatiotemporal resolution available for revealing meso-scale features (Le Traon and Dibarboure, 1999; Pascual *et al.*, 2006; Chelton *et al.*, 2011). The initial GVA data were mapped onto a 1/3˚ Mercator grid and then bilinearly interpolated onto a 0.25˚×0.25˚ longitude/latitude grid to well identify eddies (Appendix A.2 of Chelton *et al.* (2011)).

On each daily GVA data map, meso-scale eddies were identified using the algorithm recently developed by Nencioli *et al.* (2010). This algorithm is based on the minimum velocity around an eddy center as the tangential velocity of an eddy increases approximately linearly with the distance from the eddy center, and reaches the maximum before decaying. The concept requires the specification of two parameters: the first parameter, a, is the minimum grid points needed to calculate the maximum tangential velocity; the second parameter, b, the domain range to obtain the local minimum velocity. In this paper, a=3 and b=2 are chosen according to the resolution of the velocity data. Assuming that all the eddies have a circular shape, and each long-lived eddy exists over 30 d, the center, shape, and equivalent radius (R_E) of an eddy can be obtained from this algorithm.

2.2 Argo Data Set and Classification of the Argo Profiles

The NPSTMW characteristics were investigated using the autonomous CTD profiling floats from the Argo program (http://www.usgodae.org/cgi-bin/argo_select.pl). This dataset spans the same temporal period as the altimetry product (between January 2002 and February 2011). The original delayed dataset is provided by 492 distinct floats from which 32245 CTD profiles were obtained during the study period. All the data were automatically preprocessed and quality controlled by the Argo data center (Wong *et al.*, 2003; Böhme and Send, 2005; Owens and Wong, 2009). The pressure, temperature and salinity data in the profiles, if not all flagged with 1, were excluded in the analysis. To investigate the characteristics of the NPSTMW, only those profiles with the shallowest record at less than 10 m layer and the deepest one below 1000 m were considered. Once selected, each profile was visually checked and those with a questionable T/S diagram were removed. The final dataset contains 20695 profiles, accounting for 64% of the initial dataset. The final T/S profiles were interpolated at a 1-dbar interval using the Akima spline method (Akima, 1970). The potential temperature (θ), the potential density (σ_θ) and the dynamic height (DH) relative to the 1000 m reference depth were computed. The anomalies of these variables (θ', S', σ_θ', DH'), treated as the meso-scale perturbations, are computed by removing the climatological profiles, which were obtained by interpolating the Ishii monthly objective analy-

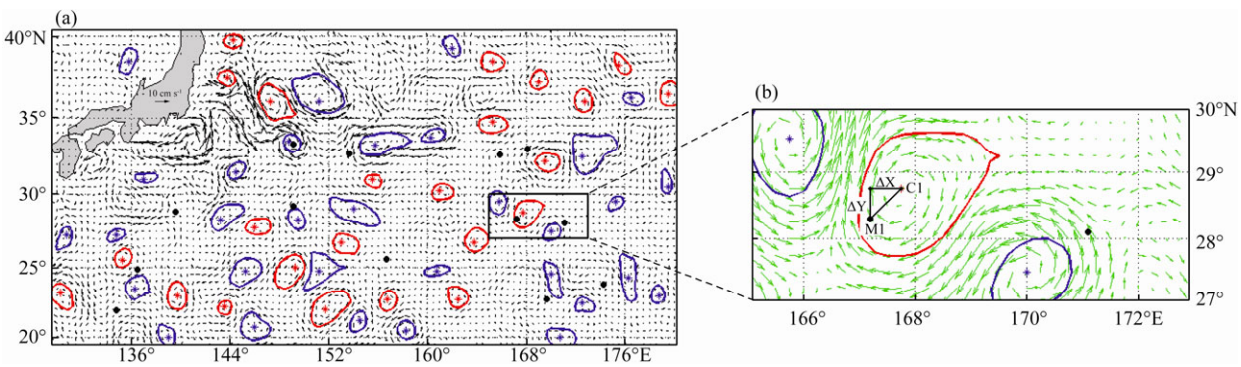

Fig.1 (a) An illustration of the eddy detection algorithm and the classification of Argo profiles. Vectors correspond to GVA (in cm s^{-1}) and black dots indicate the locations of Argo profiles on 14 August, 2008. The edges of the automatically identified cyclonic and anticyclonic eddies are represented by blue and red contours, respectively. (b) The float position (M1) relative to the corresponding eddy center (C1); this eddy-centered referential (ΔX, ΔY), which is normalized by dividing the corresponding eddy radius, is used to construct the composite eddies through the objective interpolation (see Fig.3 and the text for details).

sis dataset (version 6.9) (Ishii *et al.*, 2005, 2009).

The 20695 profiles were classified into three distinct categories according to the float location inside or outside an eddy. In order to exclude the influence of the eddy size, the dimensionless distance, $D_n=D/R_E$, was calculated, where D represents the zonal (ΔX) or meridional distance (ΔY) between a profile and the corresponding eddy. Those profiles within twice radius of the nearest CEs (AEs) were used to construct the CE (AE). The results of the classification and the distance for a given day (14 August 2008) are shown in Fig.1.

3 Results and Conclusion

3.1 NPSTMW Thickness in CEs and AEs

By following the definition by Suga *et al.* (1989), the potential vorticity is calculated as

$$Q=-(f/\rho)\cdot(\partial\sigma_\theta/\partial z)\,,$$

where f is the Coriolis parameter, and ρ the in situ density. The NPSTMW is defined as the water with PV less than $1.5\times10^{-10}\,\mathrm{m^{-1}\,s^{-1}}$, θ between 16°C and 19.5°C, and the density σ_θ between 25.0 and 25.6 $\mathrm{kg\,m^{-3}}$. Based on the definition, the thickness of NPSTMW (H) on each Argo profile, with the mixed layer depth (defined as the depth at which the density was 0.03 $\mathrm{kg\,m^{-3}}$ heavier than that at the 10-m depth (Weller and Plueddemann, 1996)) excluded, was calculated. The low-Q layers with the thickness less than 25 dbar and existing only at depths less than 100 dbar were regarded as small-scale features and were excluded (Oka *et al.*, 2011). In order to investigate the differences of H between CEs and AEs, the time series of H and its standard deviation in each category are plotted in Fig.2. Only the Argo profiles to the north of 27°N were taken into account, because the NPSTMW thickness to the south of 27°N was too small (the NPSTMW was identified on only 17% of the profiles and less than 0.1% of the profiles had an H exceeding 150 dbar). Hereafter the eddies will only refer to those to the north of 27°N. The average H of AEs is about 60 dbar thicker than that of CEs. The NPSTMW thicker than 150 dbar in AEs accounts for 18%, whereas that in CEs accounts for only 1% (Fig.2 and Table 1). Fig.2 and Table 1 show that the anticyclonic eddies provide favorable conditions for the NPSTMW intensification comparing to the cyclonic eddies. Uehara *et al.* (2003) studied the statistical relationships of H and 12°C isotherm depth (thermocline) and found that anticyclonic eddies correspond to thicker NPSTMW.

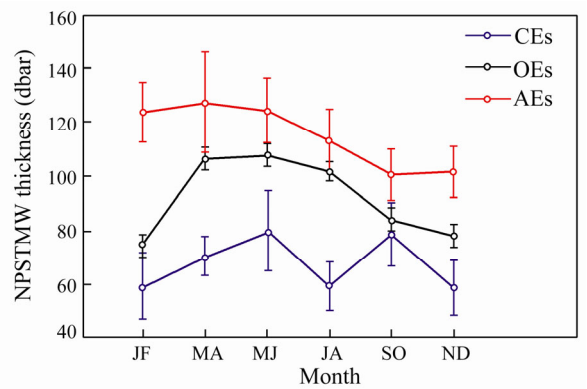

Fig.2 The NPSTMW thickness (H) on Argo profiles in CEs, AEs and OEs at a bi-monthly interval. The open-circles and bars denote the averages and bootstrapped 95% confidence intervals, respectively.

Table 1 NPSTMW thickness distributions of different categories: in cyclonic eddies (CEs), in anti-cyclonic eddies (AEs) and outside eddies (OEs)

Month	OEs			CEs			AEs		
	Initial	≥25 dbar	≥150 dbar	Initial	≥25 dbar	≥150 dbar	Initial	≥25 dbar	≥150 bar†
Jan–Feb	1670	525	39	136	24	1	78	27	7
Mar–Apr	1791	925	221	104	47	0	121	70	24
May–Jun	1833	1028	262	154	46	5	173	124	39
Jul–Aug	1922	975	213	181	33	1	172	128	39
Sep–Oct	1848	856	99	123	34	0	138	97	20
Nov–Dec	1867	714	71	118	22	0	134	73	25
Total	10921	5023	1165	816	206	7	816	519	154

Notes: † The thickness of NPSTMW greater than 150 dbar. Initial: the Argo profiles of different categories to the north of 27°N.

3.2 Composite Eddies

The Argo profiles with a normalized all direction distance of less than 2 were used to construct the cyclonic or anticyclonic eddies. Assuming that all the CEs or AEs in the research area have similar 3-D structures, a coordinate system (Δx, Δy) was used to investigate the spatial distribution of a given property (anomaly) around CEs and AEs. The centers of eddies are fixed on the average latitude of the domain (32°N). Figs.3a–d show the potential temperature and salinity anomaly distributions as a function of the normalized distance (Δx, Δy). About 3377 (3517) profiles near CEs (AEs) were used to composite eddies.

At each water depth level, the property anomalies that are three times larger than the inter-quartile range from either the first or the third quartile were considered as outliers and removed from the analysis. The remaining properties (anomalies) were then mapped on a regular grid using the Cressman interpolation,

$$W_{i,j}=(R^2-r_{i,j}^2)/(R^2+r_{i,j}^2)\,,$$

where $r_{i,j}$ is the normalized distance between the profile location and the grid point, and R is the radius of influence (Cressman, 1959). Figs.3a–d show the temperature and salinity anomalies, and the corresponding interpo-

lated results at the 200 m level for CEs and 400 m for AEs, respectively.

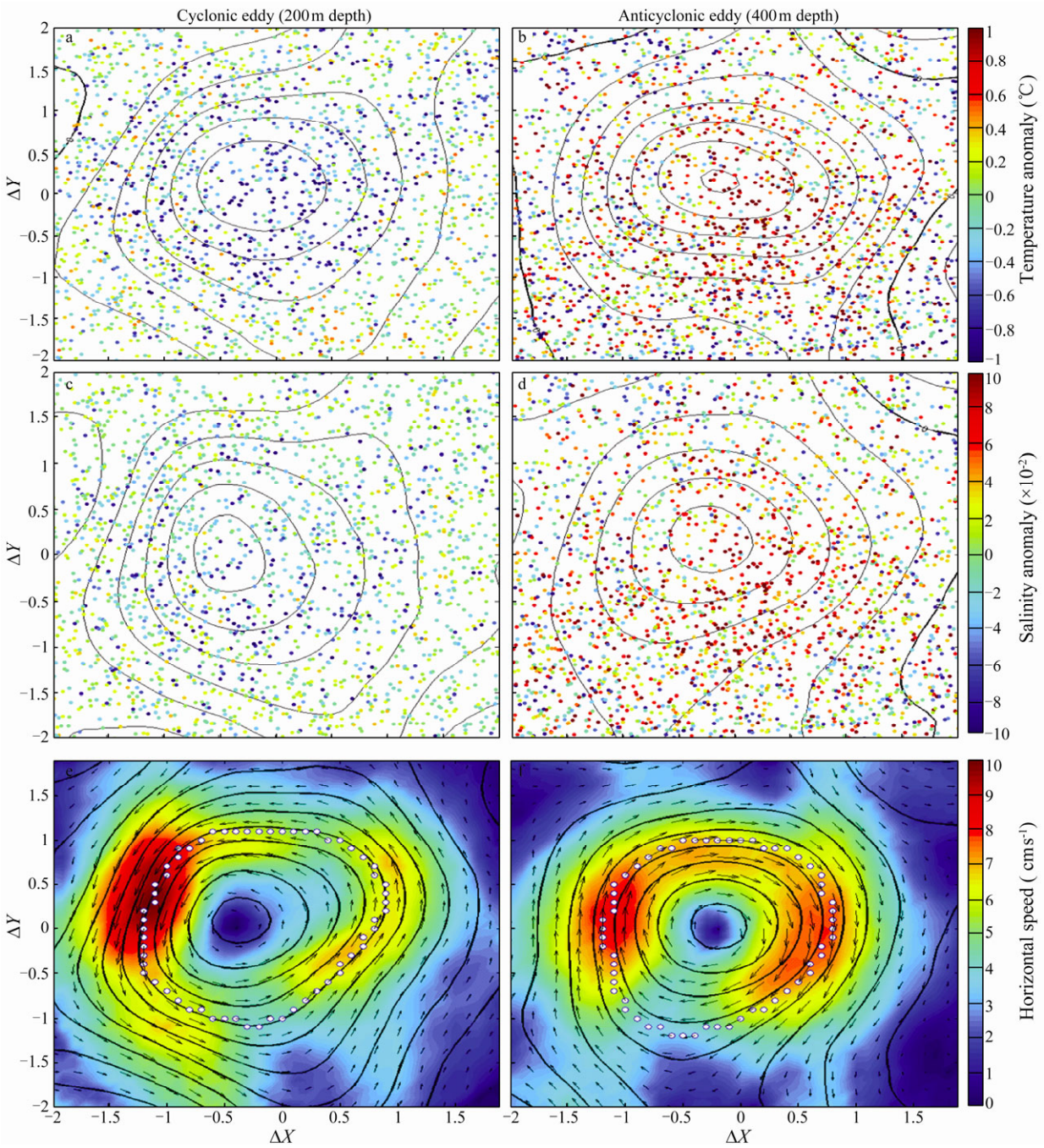

Fig.3 Objective interpolation of potential temperature anomalies (a, b) and salinity anomalies (c, d) on a dimensionless gridded domain (0.1×0.1). The anomalies are at 200 m depth and 400 m depth for cyclonic eddies (a, c) and for anticyclonic eddies (b, d), respectively. Solid dots in (a, d) show the anomalies estimated from Argo profiles in the eddy-centered referential, whereas contours correspond to the results of the objective interpolation. Black contours in (e, f) represent the objectively interpolated dynamic height anomaly at 200 m and 400 m depths relative to 1000 m, and the color shading and vectors show the corresponding horizontal geostrophic velocity (in cm s^{-1}). The composite eddy edges identified from the automatic algorithm are showed as white dots. The anomalies were computed using the Ishii climatology dataset interpolated in time and space of the Argo float data.

3.3 STMW in Composite Eddies

By using model output, Nishikawa *et al.* (2010) composited an anticyclonic eddy and claimed that the eddy can influence the STMW in two ways: eddy mixing and eddy advection. According to Qiu *et al.* (2006), the STMW intensity can be calculated as the vertically integrated PV anomaly (relative to Q_0=1.5×10^{-10} m^{-1} s^{-1}) over the STMW layer:

$$I = \int_{z_2}^{z_1} [Q_0 - Q(z)] \mathrm{d}z ,$$

where z_1 and z_2 are the upper and lower boundaries of the STMW layer with $Q<Q_0$. In general, the NPSTMW is observed to be more (less) intense toward the center of the composite AE (CE) than along its edges (Figs.4a–b). And Figs.4e–f show that the low-PV core has a convex (concave) shape in the vertical PV section across an AE (CE). It is clear that the AE traps and transports the low-PV water to the south (Figs.4c–d), which confirms the eddy advection mechanism reported by Nishikawa *et al.* (2010). But the Argo data do not verify the eddy mixing mechanism because of the insufficient data and the briefness of an eddy mixing process.

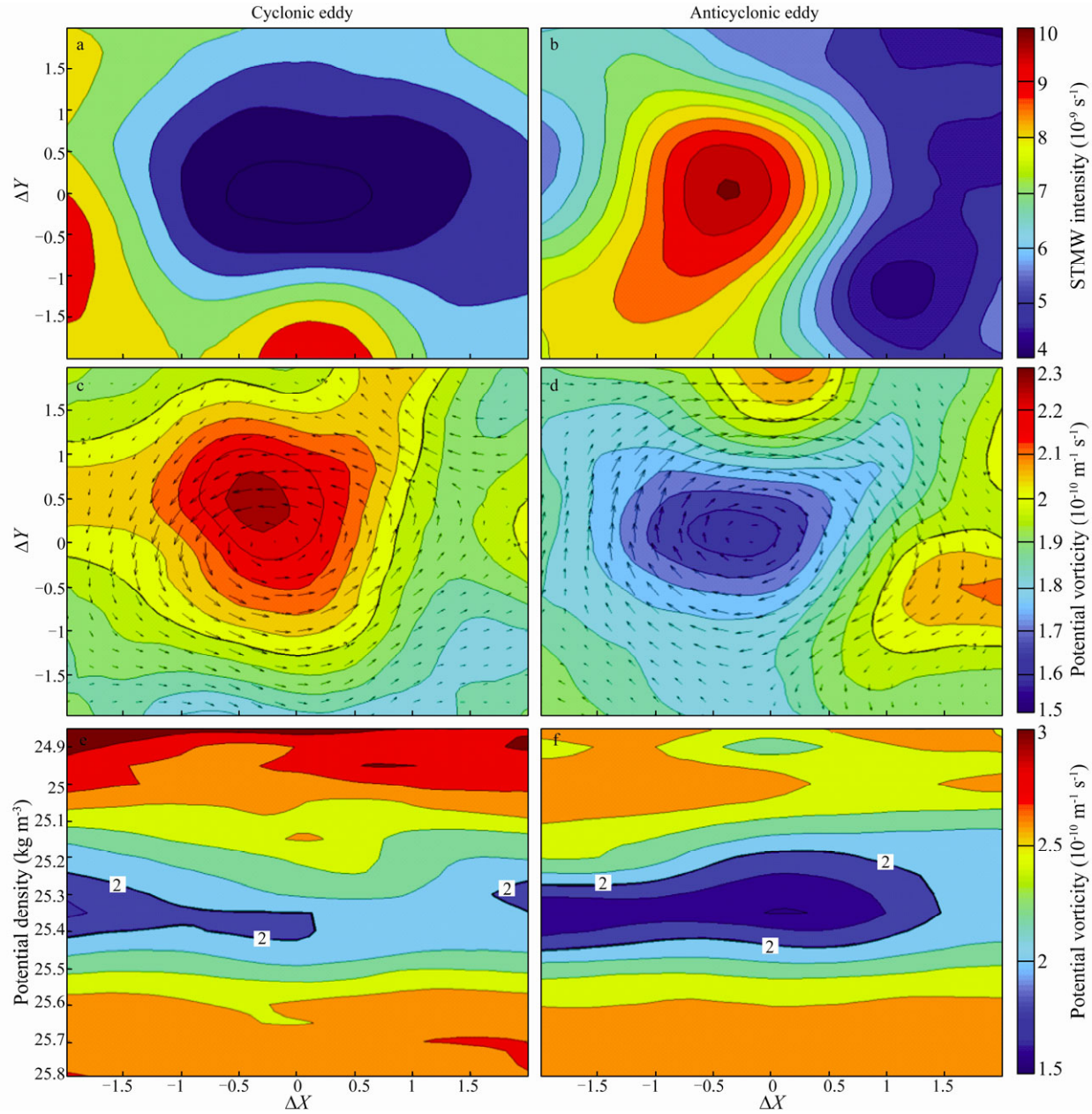

Fig.4 The low PV water in the composite CE and AE constructed by the Argo profiles between May and December. The intensity of STMW in the CE and AE is shown in a) and b), respectively. c) and d) show the composite PV in the CE and AE. The arrows denote the composite horizontal vectors on σ_θ=25.25. The vertical sections of PV in the CE and AE are displayed in e) and f), and the black thick line denotes the 2.0×10^{-10} m^{-1} s^{-1} contour.

3.4 Vertical Extent of the Trapped Fluid

The above analysis has indicated that the anticyclonic eddies provide more favorable conditions for the formation of a thicker NPSTMW. Suga (1995) presented a direct evidence of the transportation of the thick NPSTMW by the AE. One of the main objectives of this study is to investigate how the anticyclonic eddies maintain the NPSTMW with negative PV anomalies. The water mass anomalies in an eddy can only be maintained if the water mass in the eddy is trapped for a considerable part, preventing surrounding water from entering the eddy when the eddy is translated (Flierl, 1981; van Aken *et al.*, 2003). Thus to reveal the influence of AEs and CEs on the NPSTMW, the part of the water column that is effectively trapped and transported by eddies should be considered.

According to Flierl (1981), the transport of the trapped water column inside a ring depends upon the translation and swirling speed. A dimensionless parameter, representing the ratio of the fluid speed to the drift speed provides a measurement of the nonlinearity of an eddy. When the parameter is greater than 1, the eddy dynamics is nonlinear and can maintain a coherent structure as the eddy translates (Flierl, 1981; Chelton *et al.*, 2007, 2011; Chaigneau *et al.*, 2011).

The swirling speeds of composite eddies at each level are characterized by the maximum average geostrophic speeds along all the closed contours of DH' inside eddies. Figs.3e and 3f show the composite DH' at 200 m (400 m) of CEs (AEs), and the corresponding geostrophic velocity derived from the slopes of DH'. The closed DH' contours associated with the strongest average rotational velocity correspond to the composite eddy-core edges (white dots in the Figs.3e and 3f). The translation speed was defined as 4.6 cm s^{-1}, which corresponds to the mean propagation speed of long-lived eddies in the study region. The ratio, derived from swirling and drifting speed, was auto-computed from surface to 1000 dar (Fig.5). It is clear that the 'trapped depth', the maximum depth where the rotational speed exceeds the translation speed, is 300 m and 500 m in the composite CE and AE, respectively. That is to say the AEs are more favorable to the formation of larger NPSTMW, can trap more NPSTMW, and thus play a more important role in the southward transport of NPSTMW comparing to the CEs.

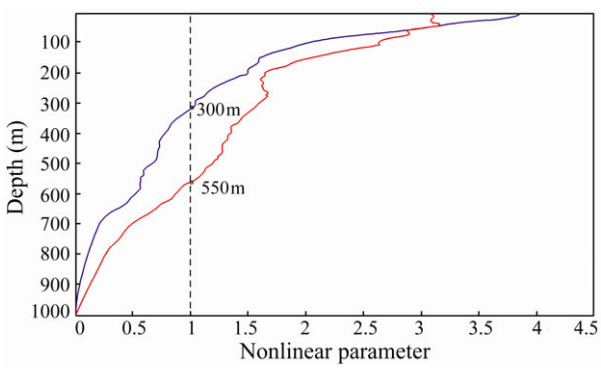

Fig.5 Vertical profiles of the swirl velocity averaged over the composite cyclonic (blue) and anticyclonic (red) eddy edges. The nonlinear parameter is obtained using the mean drift velocity of 4.6 cm s^{-1}. The indicated depths correspond to the vertical extent of trapped water within the composite eddies (300 m for CEs and 550 m for AEs).

3.5 Discussion and Conclusion

By using the velocity-based eddy detecting algorithm and the Argo profiles, thousands of AEs and CEs are identified and classified based on profile locations relative to an eddy. About 816 profiles in the cyclonic and 816 profiles in the anticyclonic eddies are obtained to the north of 27°N and some derived quantities, such as the thickness of NPSTMW, computed. The mean H of AEs is about 60 dbar thicker than that of CEs. The NPSTMW thicker than 150 dbar in AEs accounts for 18%, whereas that in CEs accounts for only 1%. Previous studies attributed the NPSTMW differences in CEs and AEs mostly to the MLD differences due to later winter conditions. But the dissipation and transportation of NPSTMW will also influence the distribution of the NPSTMW. Thus, the Argo profiles near eddies are used to composite the AEs and CEs and the vertical extent of the trapped fluid in each composite eddy is examined. By tracking the water depth where the rotational speed exceeds transitional speed of composite eddies, it is found that AEs can trap and transport water from the surface to the 550 m depth, but CEs can only extend to the 300 m depth. In other words, more NPSTMW with high PV anomalies is trapped in AEs than in CEs, which prevents surrounding water from entering the eddy and destroying the uniform structure of NPSTMW in eddies.

Results of previous climate modeling studies showed a stronger mode water and a more southward intrusion than the observations, and thus exaggerated the mode water dynamics in the subtropical countercurrent (Xie *et al.*, 2011). It is also noted that the thickness of NPSTMW suddenly drops near 27°N in both this investigation and previous studies (see Fig.2 of Oka *et al.* (2011)), which implies that the NPSTMW could experience great diffusion because its southward transport is carried by eddies. Therefore, clarifying the NPSTMW diffusion as it moves southward will be one of the most important topics in future studies.

Acknowledgements

This work was supported by the National Basic Research Program of China (Grant No. 2012CB955602) and the National Natural Science Foundation of China (Grant Nos. 41076005 and 41176009). The authors benefited from discussions with Drs. S.-P. Xie, A. Chaigneau, and Prof. Q. Liu. Constructive comments from anonymous reviewers greatly helped improve the manuscript. We also thank Y. Li for improving the manuscript.

References

Akima, H., 1970. A new method of interpolation and smooth curve fitting based on local procedures. *Journal of the Association for Computing Machinery*, **17**: 589-603.

Bingham, F. M., 1992. Formation and spreading of subtropical mode water in the North Pacific. *Journal Geophysical Research*, **97**: 11177-11189.

Böhme, L., and Send, U., 2005. Objective analyses of hydrographic data for referencing profiling float salinities in highly variable environments. *Deep Sea Research Part II*, **52**: 651-664.

Chaigneau, A., Le Texier, M., Eldin, G., Grados, C., and Pizarro, C., 2011. Vertical structure of mesoscale eddies in the eastern South Pacific Ocean: A composite analysis from altimetry and Argo profiling floats. *Journal Geophysical Research*, **116**, C11025, DOI: 10.1029/2011JC007134.

Chelton, D. B., Schlax, M. G., and Samelson, R. M., 2011. Global observations of nonlinear mesoscale eddies. *Progress in Oceanography*, **91**: 167-216.

Chelton, D. B., Schlax, M. G., Samelson, R. M., and de Szoeke, R. A., 2007. Global observations of large oceanic eddies. *Geophysical Research Letters*, **34**, L15606, DOI: 10.1029/2007GL030812.

Cressman, G. P., 1959. An operational objective analysis system. *Monthly Weather Review*, **87**: 367-374.

Flierl, G. R., 1981. Particle motions in large-amplitude wave fields. *Geophysical Journal of the Royal Astronomical Society*, **18**: 39-74.

Ishii, M., and Kimoto, M., 2009. Reevaluation of historical ocean heat content variations with time-varying XBT and MBT depth bias corrections. *Journal of Oceanography*, **65** (3): 287-299.

Ishii, M., Shouji, A., Sugimoto, S., and Matsumoto, T., 2005. Objective analyses of SST and marine meteorological variables for the 20th century using COADS and the Kobe Collection. *International Journal of Climatology*, **25** (7): 865-879.

Kouketsu, S., Tomita, H., Oka, E., Hosoda, S., Kobayashi, T., and Sato, K., 2012. The role of meso-scale eddies in mixed layer deepening and mode water formation in the western North Pacific. *Journal of Oceanography*, **68**: 63-77.

Le Traon, P. Y., and Dibarboure, G., 1999. Mesoscale mapping capabilities from multiple altimeter missions. *Journal of Atmospheric & Oceanic Technology*, **16**: 1208-1223.

Masuzawa, J., 1969. Subtropical mode water. *Deep Sea Research*, **16**: 463-472.

Nencioli, F., Dong, C., Dickey, T., Washburn, L., and McWilliams, J., 2010. A vector geometry based eddy detection algorithm and its application to high-resolution numerical model products and High-Frequency radar surface velocities in the Southern California Bight. *Journal of Atmospheric & Oceanic Technology*, **27** (3): 564-579.

Nishikawa, S., Tsujino, H., Sakamoto, K., and Nakano, H., 2010. Effects of mesoscale eddies on subduction and distribution of subtropical mode water in an eddy-resolving OGCM of the western North Pacific. *Journal of Physical Oceanography*, **40**: 1748-1765.

Oka, E., Suga, T., Sukigara, C., Toyama, K., Shimada, K., and Yoshida, J., 2011. 'Eddy-resolving' observation of the North Pacific subtropical mode water. *Journal of Physical Oceanography*, **41**: 666-681.

Owens, W. B., and Wong, A. P. S., 2009. An improved calibration method for the drift of the conductivity sensor on autonomous CTD profiling floats by θ-S climatology. *Deep Sea Research Part I*, **56**: 450-457.

Pascual, A., Faugère, Y., Larnicol, G., and Le Traon, P. Y., 2006. Improved description of the ocean mesoscale variability by combining four satellite altimeters. *Geophysical Resserch Letters*, **33**, L02611, DOI: 10.1029/2005GL024633.

Qiu, B., and Chen, S., 2006. Decadal variability in the formation of the North Pacific subtropical mode water: Oceanic versus atmospheric control. *Journal of Physical Oceanography*, **36**: 1365-1380.

Qiu, B, Hacker, P., Chen, S., Donohue, K. A., Watts, D. R., Mitsudera, H., Hogg, N. G., and Jayne, S. R., 2006. Observations of the subtropical mode water evolution from the Kuroshio Extension System Study. *Journal of Physical Oceanography*, **36**: 457-473.

Qu, T., Xie, S. P., Mitsudera, H., and Ishida, A., 2002. Subduction of the North Pacific mode waters in a global high-resolution GCM. *Journal of Physical Oceanography*, **32**: 746-763.

Rainville, L., Jayne, S. R., McClean, J. L., and Maltrud, M. E., 2007. Formation of subtropical mode water in a high-resolution ocean simulation of the Kuroshio Extension region. *Ocean Modelling*, **17**: 338-356.

Suga, T., and Hanawa, K., 1995. The subtropical mode water circulation in the North Pacific. *Journal of Physical Oceanography*, **25**: 958-970.

Suga, T., Hanawa, K., and Toba, Y., 1989. Subtropical mode water in the 137°E section. *Journal of Physical Oceanography*, **19**: 1605-1618.

Suga, T., Motoki, K., Aoki, Y., and Macdonald, A. M., 2004. The North Pacific climatology of winter mixed layer and mode waters. *Journal of Physical Oceanography*, **34**: 3-22.

Uehara, H., Suga, T., Hanawa, K., and Shikama, N., 2003. A role of eddies in formation and transport of North Pacific Subtropical Mode Water. *Geophysical Resserch Letters*, **30** (13), 1705, DOI: 10.1029/2003GL017542.

van Aken, H., van Veldhoven, A. K., Veth, C., de Ruijter, W. P. M., van Leeuwen, P. J., Drijfhout, S. S., Whittle, C. P., and Rouault, M., 2003. Observations of a young Agulhas ring, Astrid, during MARE in March 2000. *Deep Sea Research Part II*, **50**: 167-195.

Weller, R. A., and Plueddemann, A. J., 1996. Observations of the vertical structure of the oceanic boundary layer. *Journal Geophysical Research*, **101** (C4): 8789-8806.

Wong, A. P. S., Johnson, G. C., and Owens, W. B., 2003. Delayed-mode calibration of autonomous CTD profiling float salinity data by climatology. *Journal of Atmospheric & Oceanic Technology*, **20**: 308-318.

Xie, S. P., Xu, L. X., Liu, Q., and Kobashi, F., 2011. Dynamical role of modewater ventilation in decadal variability in the central subtropical gyre of the North Pacific. *Journal of Climate*, **24**: 1212-1225.

(Edited by Xie Jun)